Volume 54
Number 22
14 June 2025
Pages 8715-9100

Dalton Transactions

An international journal of inorganic chemistry

rsc.li/dalton

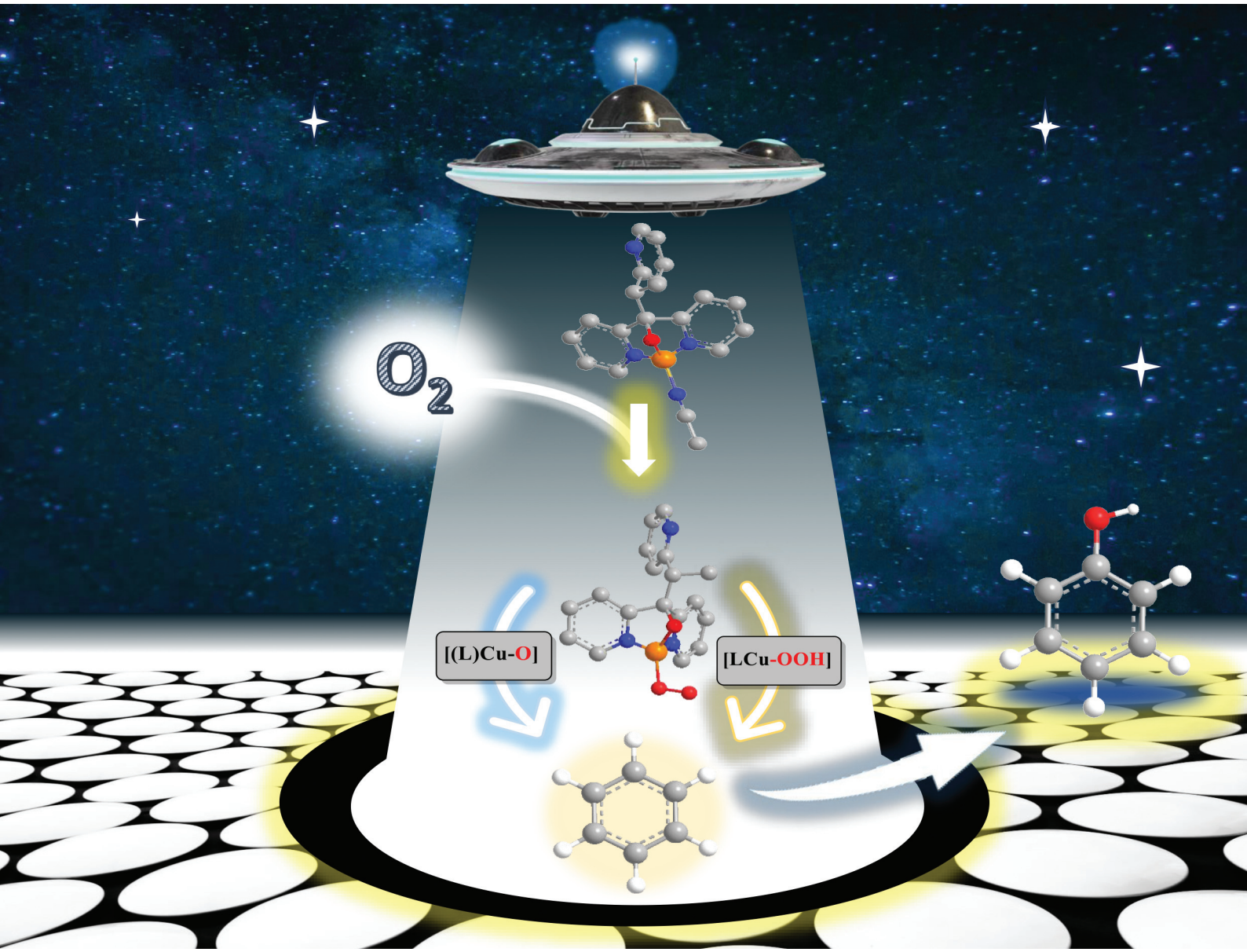

ISSN 1477-9226

ROYAL SOCIETY OF CHEMISTRY

PAPER

Ramasamy Mayilmurugan *et al.*

A bioinspired model for copper monooxygenase: direct aromatic hydroxylation using O_2

Dalton Transactions

ROYAL SOCIETY OF CHEMISTRY

PAPER

View Article Online
View Journal | View Issue

Cite this: *Dalton Trans.*, 2025, **54**, 8788

A bioinspired model for copper monooxygenase: direct aromatic hydroxylation using O_2†

Ramamoorthy Ramasubramanian, [a,b] Karunanithi Anandababu, [a,b] Mukesh Kumar [c] and Ramasamy Mayilmurugan *[a,d]

A novel copper(I) complex, $[Cu^{I}(L)(CH_3CN)]CF_3SO_3$ (**1**) (L = 1,1,2-tri(pyridin-2-yl)propan-1-ol), has been synthesized, characterized, and investigated as a bioinspired model for copper monooxygenases. Under aerobic conditions in CH_3CN, complex **1** undergoes conversion to a dicopper complex, $[(Cu^{II}L)(Cu^{II}L\ H)(SO_3CF_3)_2]\cdot CF_3SO_3\cdot H_2O$ (**2**), whose molecular structure reveals a Cu–Cu distance of 2.96 Å. A dicopper(II) complex, $[(LCu^{II})_2(SO_3CF_3)_2]$ (**3**), has been synthesized for comparison, which exhibits a similar Cu–Cu distance of 2.97 Å. EPR spectroscopy has ascertained the solution-state geometries of complexes **2** and **3**, which displayed $g_{\parallel} > g_{\perp}$ values, indicative of distorted square pyramidal geometries consistent with their solid-state structures. Complex **1** selectively hydroxylates benzene in the presence of O_2 and Et_3N, affording 7% phenol based on the substrate, without any side products. However, the use of H_2O_2 as the oxygen source under identical conditions significantly increases the phenol yield to 19%. The catalytically active intermediates generated by the reaction of complex **1** with dioxygen showed an O ($\pi^*\sigma$) → Cu ligand-to-metal charge transfer (LMCT) transition at 360 nm and a d–d transition at 650 nm. These spectral features are more pronounced with H_2O_2, showing a new LMCT transition at 360 nm and a very weak d–d transition at 689 nm. This is supported by solution FT-IR spectroscopy, which showed an O–O stretching frequency at 890 cm^{-1} (DFT spectra at 829 cm^{-1}), corresponding to a Cu–OOH intermediate. The structure of the $[(L)Cu^{II}–OOH]^+$ species was optimized by DFT calculations. Kinetic isotope effect (KIE) studies using C_6H_6/C_6D_6 (1 : 1) (k_H/k_D = 1.03) and isotopic labeling experiments using $H_2{}^{18}O_2$ support our proposed mechanism of benzene hydroxylation. In contrast, dinuclear complexes **2** and **3** exhibited poor benzene hydroxylation activity even with H_2O_2 and yielded only 4% and 6% phenol, respectively, along with by-products such as biphenyl and quinone under identical conditions.

Received 19th July 2024,
Accepted 19th April 2025

DOI: 10.1039/d4dt02079k

rsc.li/dalton

Introduction

One of the most challenging reactions so far in the arena of chemistry is the selective C–H functionalization of aromatic hydrocarbons using greener oxidants like O_2,[1–5] H_2O_2,[6–11] and N_2O[12,13] in a single step. In nature, a class of metalloenzymes selectively activates aromatic C–H bonds by utilizing metal-bound oxygen species as crucial catalytic intermediates. These oxygenation reactions are known to play a vital role in the biological metabolism of many living organisms,[14–19] which includes monooxygenase and hydroxylase types of enzymes. Their bioinorganic components have been well documented over the decades by several researchers.[20–24] Of particular interest, non-heme copper monooxygenase enzymes such as particulate methane monooxygenase (pMMO),[15,16,25] dopamine β-monooxygenase (DβM),[17–19] tyrosinase (Ty),[21,26] tyramine β-monooxygenase (TβM), peptidylglycine-α-hydroxylating monooxygenase (PHM), and polysaccharide monooxygenase (PMO) play a crucial role in the functionalization of challenging C–H bonds using dioxygen. They use specially adapted structural motifs to activate O_2 and enable selective C–H functionalization. These enzymes utilize copper centers to elegantly facilitate oxygenation/oxidation reactions of various hydrocarbon substrates under ambient conditions.[15–21] Nevertheless, selective aromatic hydroxylation is challenging and is consistently found to be an enduring area of interest in bioinspired catalysis research. In particular, a direct synthetic methodology for the aromatic hydroxylation of hydrocarbons has not been well explored. Hydroxylated hydrocarbons are

[a]*Department of Chemistry, Indian Institute of Technology Bhilai, Bhilai, Durg 491002, Chattisgarh, India. E-mail: murugan@iitbhilai.ac.in*
[b]*Department of Chemistry, National Sun Yat-sen University, Kaohsiung, 80424, Taiwan*
[c]*Radiation Biology and Health Sciences Division, Bhabha Atomic Research Centre, Mumbai, Maharashtra 400 085, India*
[d]*Department of Bioscience and Biomedical Engineering, Indian Institute of Technology Bhilai, Bhilai, Durg 491002, Chattisgarh, India*

†Electronic supplementary information (ESI) available. CCDC 1962712 and 1962738. For ESI and crystallographic data in CIF or other electronic format see DOI: https://doi.org/10.1039/d4dt02079k

synthetic precursors for many drugs and polymer materials. Phenol is one such valuable compound, and it is produced commercially worldwide by a three-step cumene process, which was developed by Hock and Lang in 1944.[5] This process has a few inherent drawbacks, such as being a multi-step process, requiring high energy consumption, and affording a poor yield of phenol (5%) along with a significant amount of acetone as a by-product. At the same time, over-oxidation of phenol is facile under oxidation conditions because phenol is more sensitive than benzene, as it lacks kinetic control.[27,28]

The earlier reports by Karlin and co-workers have focused mainly on intramolecular hydroxylation on auxiliary ligands or electron-rich aromatic systems using bioinspired models of tyrosinase, in which various copper complexes and their reactive intermediates were extensively studied.[4,29,30] In 2011, Perez and co-workers reported [Tp^{x}Cu(NCMe)] [Tp^x = hydrotris(pyrazolyl)borate] as a catalyst for benzene hydroxylation. They achieved a phenol yield of 21%, but with poor selectivity (phenol : benzoquinone = 70 : 30) at 80 °C, and no deeper mechanistic investigation was reported.[31] Later, in 2017 and 2022, the same group proposed two mechanisms (rebound or electrophilic substitution) through a Wheland intermediate for benzene hydroxylation *via* experimental and DFT studies.[32,33] In 2017, Kodera and co-workers explored benzene hydroxylation using a dicopper(II) complex [Cu$_2$(μ-OH)6-hpa]$^{3+}$ [hpa = 2-bis(2-pyridylmethyl)aminomethyl-6-pyridylethane] as the catalyst and achieved 22% conversion of benzene into phenol.[34] The mechanism of the oxidation of benzene to phenol with H_2O_2 by copper complexes is still unclear in the literature, such as whether the reaction proceeds directly *via* a Cu–oxygen species or indirectly *via* radical species produced by Cu–oxygen species. Our group has developed bioinspired Cu(II) complexes with N_4 ligands and achieved a 37% phenol yield using H_2O_2, with the reaction proceeding *via* Cu(II)OOH species as an active intermediate.[35] Later, Cu(I) complexes reported by us showed benzene hydroxylation with a 29% phenol yield but with reduced selectivity compared to Cu(II) complexes.[36] All the above-reported bioinspired aromatic hydroxylation studies extensively used H_2O_2 as an oxygen source. However, none of the reports attempted to use dioxygen as an oxygen source, except for Karlin and co-workers' study of intramolecular hydroxylation on the ligand moiety.[4,29]

This article reports the synthesis of a new derivative of the tris-pyridine-based ligand[36] and its copper(I) complexes, serving as a relevant bioinspired model for copper monooxygenase enzymes. The Cu(I) complex catalyst effectively converts benzene to phenol using dioxygen as a greener source, achieving a phenol yield of 7% based on benzene. Furthermore, the yield can be enhanced to 19% when using H_2O_2. Notably, this represents one of the rare examples of intermolecular aromatic hydroxylation by a Cu(I) complex utilizing dioxygen, and only a few reports are available in the literature. Our spectral data and catalysis experiments support the idea that the benzene hydroxylation likely proceeds *via* active Cu(II)–OOH species, and the experimental results align well with the data obtained from DFT and TDDFT calculations.

Results and discussion

Synthesis and characterization

The ligand L = [1,1,2-tri(pyridin-2-yl)propan-1-ol] was synthesized from di-2-pyridyl ketone with lithiated 2-ethyl pyridine in THF at −70 °C and its formation was confirmed by NMR and ESI-MS spectral methods (Scheme 1A, Fig. S1–S3†). The copper(I) complex [Cu^I(L)(CH$_3$CN)]CF$_3$SO$_3$ **1** was synthesized by the reaction of [Cu(CH$_3$CN)$_4$]CF$_3$SO$_3$ with L (1 : 1) in a degassed toluene/acetone mixture under a strict Ar atmosphere. Its formation was confirmed by HRESI-MS, ^{1}H-NMR analysis and elemental analysis (Scheme 1B, Fig. S4 and S5†). Our repeated attempts to crystallize **1** were unsuccessful under various dry conditions. It underwent spontaneous aerial oxidation and structural rearrangements to afford a single crystal of [(Cu^{II}L)(Cu^{II}L H)(SO$_3$CF$_3$)$_2$]·CF$_3$SO$_3$·H$_2$O **2**, which has adopted a dicopper(II) complex (Fig. 1, S21,† Table 1 and Table S1†). Interestingly, one of the pyridyl arms was protonated due to an acidic environment in the solution. For comparison, the copper(II) complex [(LCu^{II})$_2$(SO$_3$CF$_3$)$_2$] **3** was synthesized by the reaction of a 1 : 1 ratio of [Cu(CF$_3$SO$_3$)$_2$] : L in acetonitrile. In fact, attempts were made to obtain a mononuclear complex; however, this always led to the formation of the dicopper(II) complex (Fig. 1, S21, Table S1† and Table 2). Complexes **2** and **3** were confirmed by HRESI-MS, EPR spectral, and single-crystal X-ray studies (Fig. S6 and S7†). However, a better understanding of the structural, spectral, and magnetic properties of **2** and **3** is needed, which is under progress.

Electronic spectral, redox, and structural properties

Complex **1** [Cu^I(L)(CH$_3$CN)]CF$_3$SO$_3$ showed π–π* transition at 383 nm (ε, 534 M^{-1} cm^{-1}) in the electronic spectra, with no detectable d–d transitions (Fig. S8†). As anticipated for a d^{10} copper(I) center, the complex is EPR silent and showed ^{1}H NMR signals at 7.31 (d, 8H), 6.75 (d, 4H), and 1.20 (m, 4H). However, due to coordination, the chemical shift values are slightly shifted from the ligand values (Fig. S5†). On the other hand, complexes **2** and **3** showed π–π* transitions at 376–379 nm along with broad d–d transitions at 686 nm (**2**, ε, 87 M^{-1} cm^{-1}) and 693 nm (**3**, ε, 159 M^{-1} cm^{-1}), respectively (Fig. S8†). The EPR spectra of **2** and **3** were recorded in a CH$_3$CN/DMF mixture at 70 K and showed an anisotropic *g*-tensor. Their hyperfine splitting due to Cu (I = 3/2) is resolved in the parallel ($g_\parallel$) region (Fig. S9†). The EPR spectra of complex **2** showed $g_\parallel$ = 2.26 and $g_\perp$ = 2.06, which are slightly shifted for **3**, $g_\parallel$ = 2.37 and $g_\perp$ = 2.05. Both the complexes exhibited $g_\parallel > g_\perp$, suggesting the presence of an odd electron located at the $d_{x^2-y^2}$ orbital. Complex **2** exhibits an *f*-value of 165 cm^{-1}, higher than the square-based geometries (105–135 cm^{-1}), indicating strong distortion in the geometry. Complex **3** showed a lower *f*-value of 125 cm^{-1}, corresponding to square-based geometry.[35,37] EPR parameters and the energies of d–d transitions were used to estimate the covalency of in-plane σ-bonds (α^2), in-plane π-bonds (β^2), and out-plane π-bonds (γ^2).[38] Complexes **2** and **3** exhibited higher α^2 (0.818–0.833), β^2 (0.928–1.08), and γ^2 (1.124–1.256) values

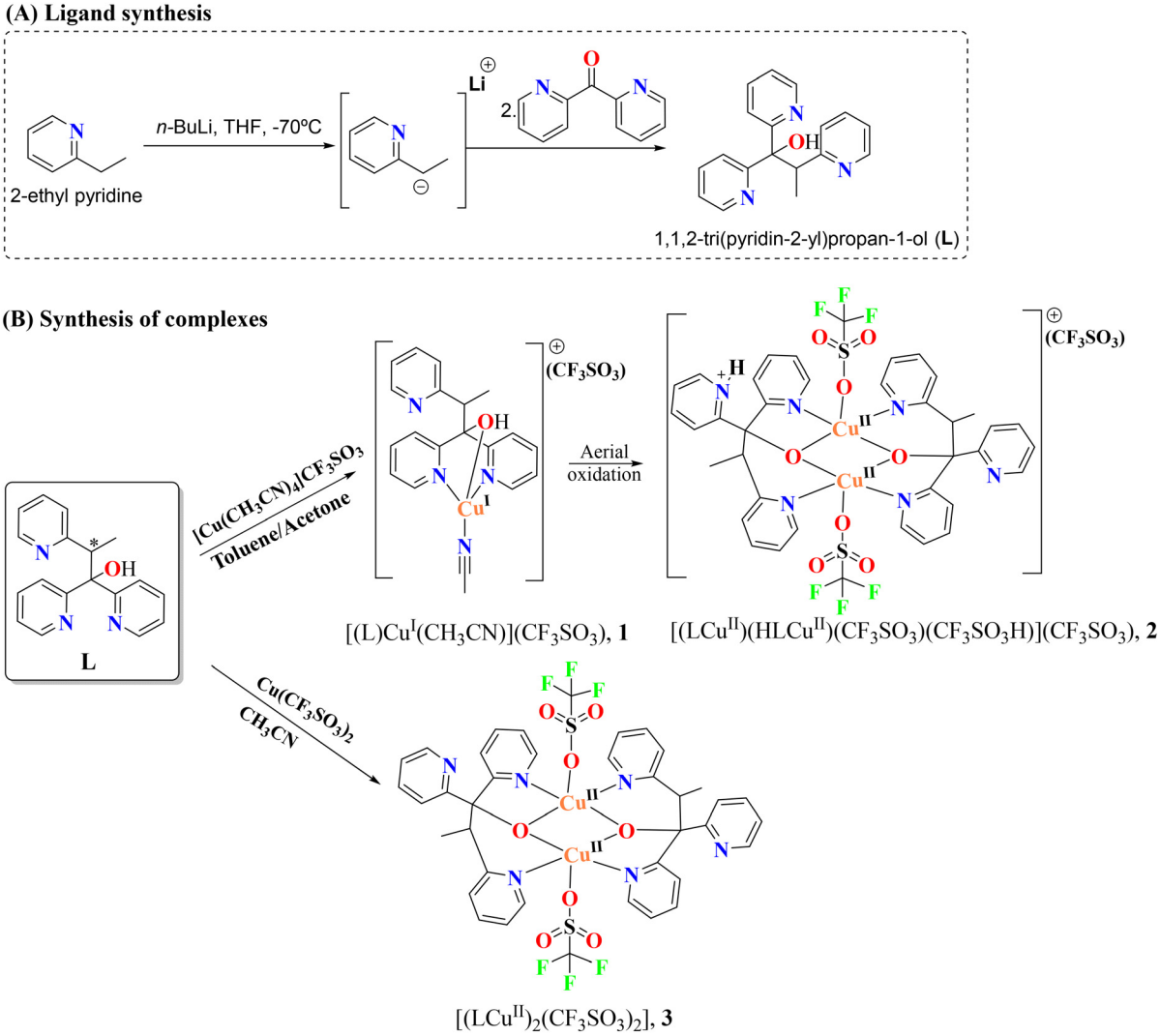

Scheme 1 Synthesis of the tris-pyridine-based ligand (L) and its copper complexes.

(Table S2†). The α^2 values indicate a slightly higher degree of in-plane σ-covalent bonding character in Cu–N bonds of **3** than that of **2**; in general, the α^2 value is close to unity for ionic bonding, and this value exhibits a reciprocal correlation with covalent character. The orbital reduction factor K for the complexes **2** ($K_{\parallel}$, 0.898; $K_{\perp}$, 0.741) and **3** ($K_{\parallel}$, 0.757; $K_{\perp}$, 0.651) was calculated, showing that $K_{\parallel} > K_{\perp}$. This reveals that the persistence of a significant amount of out-of-plane π-bonding. The pure σ-bonding $K_{\parallel} = K_{\perp}$ and $K_{\parallel} < K_{\perp}$ for π-bonding at in-plane have been described in the literature.[39,40] The Fermi contact hyperfine interaction term (K) was calculated as 0.323 and 0.363 for **2** and **3**, indicating an almost identical degree of covalent bonding character in Cu–N as predicted from α^2 values.[37] Cyclic voltammetry of **3** exhibited two reduction peaks at −0.25 V and −0.53 V *vs.* Ag/Ag^+, and their oxidation peaks are ill-defined, which are attributed to the reduction processes associated with each of the dicopper(II) centers (Fig. S10†).

The molecular structures of complexes **2** and **3** were determined by single-crystal X-ray studies. The unit cells of complexes **2** and **3** showed dicopper centres having distorted square pyramidal geometry (Fig. 1), with τ values for **2** (τ_1, 0.21; τ_2, 0.29) and **3** ($\tau_1 = \tau_2 = 0.23$).[41] The slightly varied τ-values of **2** ensure a different electronic environment enforced by the protonation of the pyridyl arm. The variation in the Cu–O bond distances reveals the asymmetric oxygen bridging between Cu1 and Cu2 centres (1.927–1.944 Å). These average Cu–O bond distances are relatively shorter than the average Cu–N_{Py} bond distances (1.965–2.026 Å) due to the strong overlapping of d-orbital Cu centers with oxygen. Also, it showed almost identical Cu–O_{otf} bond distances; this anion coordination is labile. The Cu–Cu distances of complexes **2** (2.959) and **3** (2.971 Å) are longer than those of other reported systems (2.38–2.93 Å).[42–44] Interestingly, the crystal structure of **2** showed that one of the pyridine arms is protonated, which was displaced from the coordination sphere (Fig. 1). Similarly, **3**

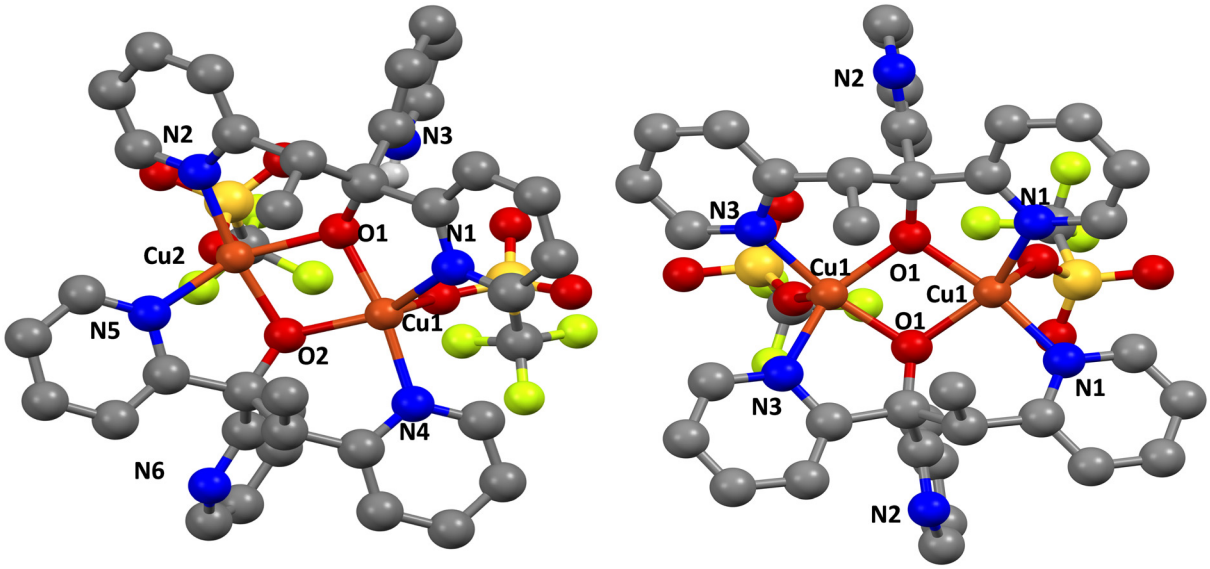

Fig. 1 Molecular structures of **2** (left) and **3** (right). (POV-Ray figures drawn from a 50% probability factor of thermal ellipsoids). For clarity, the hydrogen atoms and other counter ions are omitted.

Table 1 Selected bond distances[a] (Å) and bond angles (°) of complex **2**

2			
Cu(1)–Cu(2)	2.959(13)	Cu(2)–N(2)	1.965(5)
Cu(1)–N(1)	2.026(6)	Cu(2)–O(1)	1.965(5)
Cu(1)–O(1)	1.944(5)	Cu(2)–O(2)	1.908(5)
Cu(1)–O(2)	1.927(5)	Cu(2)–O(4)	2.292(6)
Cu(1)–O(3)	2.272(5)	Cu(2)–N(5)	2.017(6)
Cu(1)–N(4)	1.982(6)		
O(2)–Cu(1)–O(1)	79.19(8)	O(2)–Cu(2)–O(1)	79.1(2)
O(3)–Cu(1)–O(1)	87.9(2)	O(4)–Cu(2)–O(2)	91.4(2)
O(3)–Cu(1)–O(2)	99.7(2)	O(4)–Cu(2)–O(1)	102.0(2)
N(1)–Cu(1)–O(1)	81.5(2)	N(2)–Cu(2)–O(1)	91.8(2)
N(1)–Cu(1)–O(2)	150.3(2)	N(2)–Cu(2)–O(2)	169.5(2)
N(1)–Cu(1)–O(3)	101.9(3)	N(2)–Cu(2)–O(4)	95.6(2)
N(4)–Cu(1)–O(1)	170.8(2)	N(5)–Cu(2)–O(1)	150.2(2)
N(4)–Cu(1)–O(2)	91.6(2)	N(5)–Cu(2)–O(2)	81.7(2)
N(4)–Cu(1)–O(3)	94.6(2)	N(5)–Cu(2)–O(4)	101.0(2)
N(4)–Cu(1)–N(1)	106.6(2)	N(5)–Cu(2)–N(2)	104.6(3)

[a] Standard deviations are given in parenthesis.

Table 2 Selected bond distances[a] (Å) and bond angles (°) of complex **3**

3			
Cu(I)–Cu(1)^1	2.971(18)	N(1)–Cu(1)–O(2)	92.6(3)
Cu(I)–O(2)	2.386(7)	O(1)^1–Cu(1)–O(2)	93.0(2)
Cu(1)–N(1)	1.981(7)	O(1)–Cu(1)–O(2)	104.5(3)
Cu(1)–O(1)	1.933(5)	O(1)^1–Cu(1)–N(1)	170.1(2)
Cu(1)–N(3)^1	2.008(7)	O(1)–Cu(1)–N(1)	92.8(2)
		N(3)^1–Cu(1)–O(2)	97.5(3)
		N(3)^1–Cu(1)–N(1)	105.6(3)
		N(3)^1–Cu(1)–O(1)	150.6(2)
		N(3)^1–Cu(1)–O(1)^1	81.8(2)
		S(1)–O(2)–Cu(1)	145.8(5)
		C(1)–N(1)–Cu(1)	121.2(5)
		C(5)–N(1)–Cu(1)	120.2(5)
		C(8)–O(1)–Cu(1)	126.6(4)
		C(8)–O(1)–Cu(1)^1	119.7(4)
		C(14)–N(3)–Cu(1)^1	113.7(5)
		C(18)–N(3)–Cu(1)^1	126.6(6)

[a] Standard deviations are given in parenthesis.

possesses dicopper(II) centres with symmetrical coordination environments. The average bond distance of Cu–N_{py} (1.994 Å) is relatively longer than the symmetrically bridged Cu–O (1.924 Å) bond distance. The Cu–O_{Otf} bond distance (2.386 Å) is longer than other bond distances and is highly labile. The Cu–Cu distance of **3** (2.971 Å) is found to be slightly longer than that of **2** (Tables 1 and 2).[45] The Cu–Cu distances in the range of <3.0 Å are speculated to facilitate C–H activation, and this is observed in the hydroxylase or monooxygenase enzymes.[16,46–48]

Model oxygenase reaction and benzene hydroxylation

The model oxygenation reaction was carried out using benzene as a substrate, where complex **1** (0.1 mmol) and benzene (5 mmol) were reacted with excess dioxygen (O_2) in the presence of the sacrificial reducing agent Et_3N (1 : 50 : 100; complex : substrate : base) in acetonitrile. The reaction proceeded at 60 °C for 48 hours, yielding phenol as the sole product with a 7% yield, calculated based on the substrate used (Scheme 2 and Scheme S1-a†). Notably, the over-oxidation products, such as benzoquinones, or self-coupling products, such as biphenyls, were not detected, highlighting the selective hydroxylation of benzene to phenol (Fig. S11†). Increasing the temperature to 70 °C or extending the reaction time showed no improvement in phenol yield. Despite the lower phenol yield,

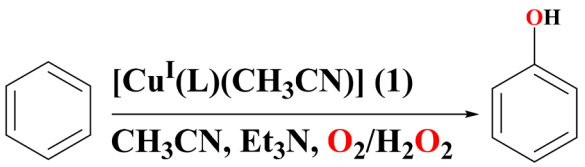

Scheme 2 Benzene hydroxylation by complex **1**.

it is interesting because intermolecular aromatic hydroxylation is rarely reported using dioxygen. Karlin and co-workers used several dicopper complexes for intramolecular hydroxylation reactions using O_2; however, direct benzene hydroxylation was rarely explored discretely.[4,29,30] Without Et_3N or a catalyst, the reaction did not yield phenol or other hydroxylation products. Therefore, Et_3N functions as a base and sacrificial reducing agent to stabilize the intermediates formed during the catalytic process. Toluene as a substrate with complex **1** under O_2 resulted in no aromatic hydroxylation; a trace of benzaldehyde was formed (>3%) at 60 °C. On the other hand, using **2** and **3** as catalysts showed no phenol formation or other products from benzene under identical conditions.

Moreover, complex **1** was investigated as a catalyst using H_2O_2 as an oxygen source to substantially enhance the yield of hydroxylation products while maintaining high selectivity for aromatic hydroxylation (Scheme 2). The reaction was optimized using 0.05 mmol of **1**, 5 mmol of C_6H_6, 5 mmol of sacrificial reducing agent Et_3N, and 25 mmol of H_2O_2 (1 : 100 : 100 : 500; complex : substrate : base : oxidant) at 60 °C in 3 mL of dry acetonitrile. The formation of product phenol was confirmed and quantified by GC-MS/GC analysis (Fig. S11†). It showed a 19% phenol yield with <99% selectivity (TON, 19) over 8 hours (Table 3).

Also, the reaction at 0–5 °C showed a trace amount of phenol formation. Meanwhile, the reaction that used phenol as a substrate exhibited no hydroxylation (catechol formation) or oxidation products. Under identical conditions, the substrate toluene (5 mmol) transformed into 9% hydroxylated products. The selectivity for aromatic hydroxylation dropped to 72% [60 : 39 : 1; o : p : m (cresols)]. Also, it showed the formation of benzoquinone derivatives (9% selectivity) and benzaldehyde (19% selectivity) as by-products (Scheme S1†). However, this result clearly reveals that aromatic hydroxylation is preferred over aliphatic hydroxylation. Similarly, using anisole as a substrate showed a 14% yield of mixed products of methoxyphenol with the selectivity of *ortho*, 55%; *meta*, 8%, and *para*, 37% (Scheme S2†). The endurance test was performed with **1** (0.1 μmol), Et_3N (10 μmol), H_2O_2 (60 mmol), and benzene (5 mmol), which yielded 1.7% of phenol over 120 hours with a maximum TON of 850 without the formation of by-products. Further increase in the reaction time did not improve the yield.

Table 3 Catalytic benzene hydroxylation[a] by **1** and H_2O_2

Complex **1** (mmol)	T^b (°C)	Oxidant (mmol)	Time (h)	S[c] (%)	Y[d] (%)	TON[e]
0.05	RT	25	8	100	12	12
0.05	**60**	**25**	**8**	**>99**	**19**	**19**
0.05	RT	10	8	100	9	9
0.05	60	10	8	>99	13	13
0.05	0–5	25	8	—	Trace	—
0.025	60	25	8	>99	9	18
0.025	60	25	30	97	21	42
0.025	60	100	8	95	19	38
0.01	60	100	12	>99	14	70
0.001	60	1000	48	>99	7	350
0.0001	**60**	**Excess**	**120**	**>94**	**1.7**	**850**
0.1	**60**	**O_2**	**48**	**>99**	**7**	**3.5[f]**

[a] Reaction conditions: benzene (5 mmol), dry Et_3N (5 mmol) and hydrogen peroxide (30%) (25 mmol) in dry acetonitrile. [b] T = temperature. [c] S = selectivity. [d] Y = yield. [e] TON = turnover number. [f] Reaction conditions: benzene (5 mmol), Et_3N (5 mmol) and excess O_2 in wet acetonitrile.

Mechanism of benzene hydroxylation

The kinetic isotopic effect (KIE) experiment was examined using a 1 : 1 ratio of $C_6H_6 : C_6D_6$ in H_2O_2 and was calculated at 25 °C, (k_H/k_D = 1.03) and 60 °C, (k_H/k_D = 1.09) from the ratio of $C_6H_5OH : C_6D_5OH$ (Fig. S12c†). It is close to the values (0.9–1.0) reported for intramolecular aromatic hydroxylation. In fact, the KIE value of ~1.0 clearly supports the involvement of metal-bound oxygen species as the key intermediate for the aromatic hydroxylation *via* an electrophilic aromatic substitution reaction.[32,49] Thus, this data excludes the involvement of the Fenton-type ($^{\bullet}OH$) reaction pathway,[50] where the KIE is reported as 1.7–1.8 or a copper-insertion type reaction.[49,51] The KIE experiment with excess dioxygen was performed in a 1 : 1 ratio of $C_6D_6 : C_6H_6$ under identical reaction conditions at 25 °C and 60 °C. The KIE value (1.01–1.09) eliminates the existence of the metal insertion C–H bond activation intermediate and proposes metal-oxo/oxyl/hydroproxo species involvement in this present study.[49,51]

Isotopic labelling experiments were performed using $H_2{}^{18}O_2$ (90% atom purity), which showed 95.3% incorporation of ^{18}O into phenol (Fig. S12a†). However, using $H_2{}^{18}O$ and H_2O_2 showed almost no ^{18}O-atom incorporation into the phenol product (Fig. S12b†). These results suggest that utilizing H_2O_2 is crucial for transforming benzene into phenol, and it is the sole source of oxygen.[52] The reaction of complex **1** (1×10^{-3} M) with H_2O_2 (5 equivalents) and Et_3N (2 equivalents) in CH_3CN under an N_2 atmosphere at −20 °C and 25 °C resulted in the formation of an O (π^*_σ) → Cu^{2+} ligand-to-metal charge transfer (LMCT) transition at 360 nm, with the observed rate constant of $(3.70 \pm 0.01) \times 10^{-2}$ s^{-1} and a lifetime (τ) of 27.02 s. Moreover, a weak d–d transition was identified at 689 nm at −20 °C, while its formation at 25 °C proceeded at a relatively slower rate (Fig. 2, S14, S15†). The low intensity of this signal is consistent with the high reactivity and instability of the Cu(II)–peroxo species, which are prone to rapid decomposition shortly after formation under the specified conditions. The identification of the O_2/H_2O_2 reaction with Cu(I)-complexes in the reaction medium presents a challenge, as observed in our system and similarly reported by other research groups.[33] Notably, the spectral features observed in this study closely resemble those attributed to the $[(L)Cu^{II}–OOH]^+$ or $[(L)Cu^{II}–O–O–Cu^{II}(L)]^{2+}$ species reported in the literature.[35,53,54] Upon treating benzene (50 equivalents) with the *in situ*-generated Cu(II)–peroxo species in acetonitrile at −20 °C, a gradual diminution of the copper–oxygen intermediate was observed. This decay is faster than its corresponding formation. The decay of the species is accompanied by a decrease in the ligand-to-metal charge transfer (LMCT) band at 360 nm, which indicates

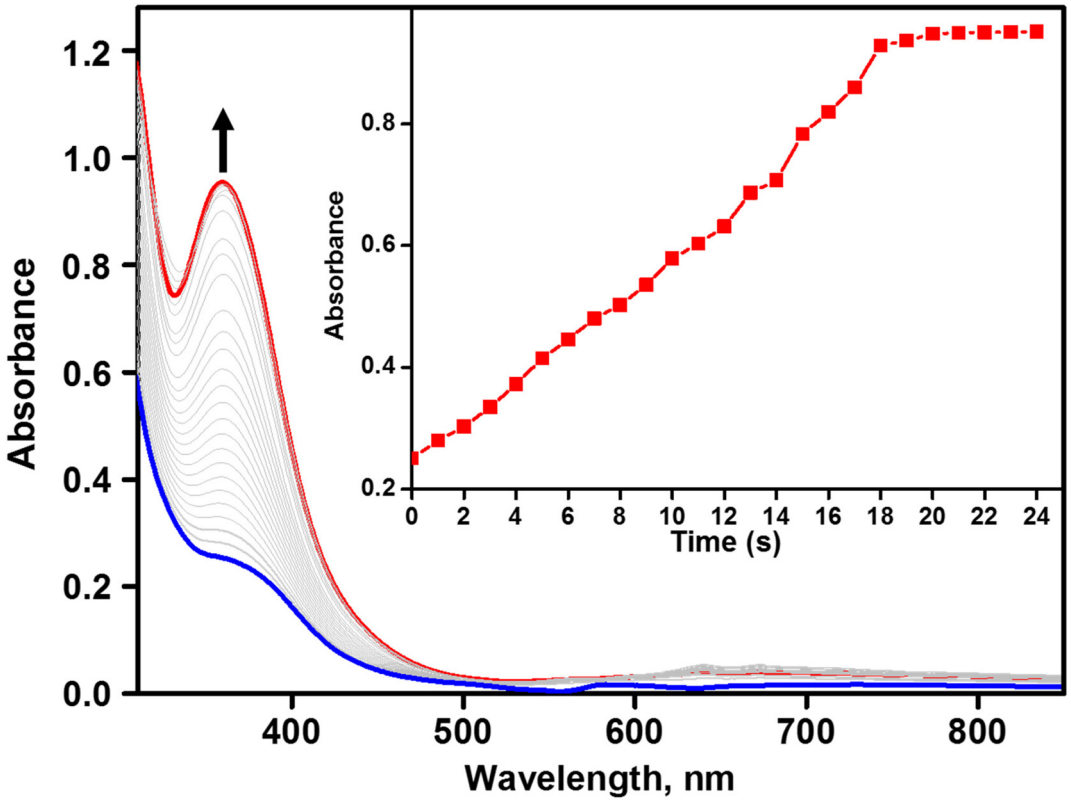

Fig. 2 Electronic spectral changes for complex **1** (1×10^{-4} M) upon reaction with 2 equivalents of Et_3N and 5 equivalents of H_2O_2 (30%) at −20 °C in dry acetonitrile. Inset: plot of time *vs.* absorbance (370 nm).

that direct transfer oxygen atom from $[(L)Cu^{II}–OOH]^+$ or *via* $[(L)Cu^{II}–O–O–Cu^{II}(L)]^{2+}$ to benzene (Fig. 4). The GCMS analysis of the reaction mixture showed that phenol was selectively formed. Similarly, exposure of complex **1** (1×10^{-3} M) to dioxygen (O_2) and Et_3N (2 equivalents) at −20 °C resulted in a comparable LMCT transition at 360 nm (743 M^{-1} cm^{-1}) and a very weak d–d transition at 670 nm (26 M^{-1} cm^{-1}) (Fig. S13†).[54–56] Thus, it suggests that $[(L)Cu^{II}–OOH]^+$ or its dimeric derivative $[(L)Cu^{II}–O–O–Cu^{II}(L)]^{2+}$ is likely to be the key intermediate for aromatic hydroxylation, as reported previously.[34–36]

Further characterization of the Cu(II)–peroxo species generated with H_2O_2 was conducted using ^1H NMR spectroscopy, which exhibited paramagnetically shifted broad signals at 11.94 (s, 2H), 10.76 (s, 2H), 8.61 (s, 4H), 7.46 (s, 3H), 6.76 (s, 2H), and 1.26 (m, 4H) (Fig. S16†). These shifts are attributed to the oxidation of Cu(I) to Cu(II). The formation of the $[(L)Cu^{II}–OOH]^+$ species was further confirmed by ESI-MS analysis, which displayed a molecular ion peak at *m*/*z* 387.0, in agreement with the calculated value (Fig. S17†). Isotopic labeling studies using $H_2{}^{18}O_2$ (90% atom purity) demonstrated a four-unit mass shift (*m*/*z* 391.0) in CH_3CN, corresponding to the formation of $[(L)Cu^{II}(^{18}O–^{18}OH)]^+$ (Fig. S17 and S18†). However, solution IR spectroscopy of $[(L)Cu^{II}–OOH]^+$ revealed vibrational bands at 890 cm^{-1} and 648 cm^{-1}, which are assigned to O–O and Cu–O stretching frequencies, respectively.[35,56] Interestingly, replacing H_2O_2 with O_2 resulted in a shift of the O–O stretching frequency to 862 cm^{-1} (Fig. 3).[4,30] It is known that Cu(II)–peroxo species typically exhibit O–O stretching frequencies within the range of 800–930 cm^{-1}.[4,30,35,56,57] The observed spectral data suggest that the species formed by the reaction of H_2O_2 may correspond to $[(L)Cu^{II}–OOH]^+$, whereas the reaction with O_2 generates a peroxo-bridged species, $[(L)Cu^{II}–O–O–Cu^{II}L]^{2+}$, with an O–O stretching frequency of 862 cm^{-1}. These vibrational spectral features are consistent with previously reported Cu(II)–oxygen species, both spectroscopically and structurally.[35,58]

Using the radical trapping reagents TEMPO and DMPO at 25 °C and 60 °C resulted in no perceptible changes in phenol yield, eliminating the possibility of a radical-type chain mechanism. On the other hand, it is known that TEMPO can also be oxidized under these conditions due to the presence of aromatic C–H bonds.[34,35,51] The oxidation of the substrate *cis*-1,2-dimethylcyclohexane was carried out under optimized reaction conditions, which showed 4.2% of the *cis*-hydroxylated product with a trace of the trans product (0.7%). This stereoretention of C–H oxidation reactions indicates that Fenton-type species are unlikely to be involved,[59] which supports our predictions by KIE studies. The benzene hydroxylation reaction in the CH_3CN–CCl_4 (5 : 1) solvent mixture exhibited the formation of a trace amount of chlorobenzene as a by-product, along with phenol (94% selectivity) as the primary product. This result suggests that CCl_4 does not affect the selectivity of

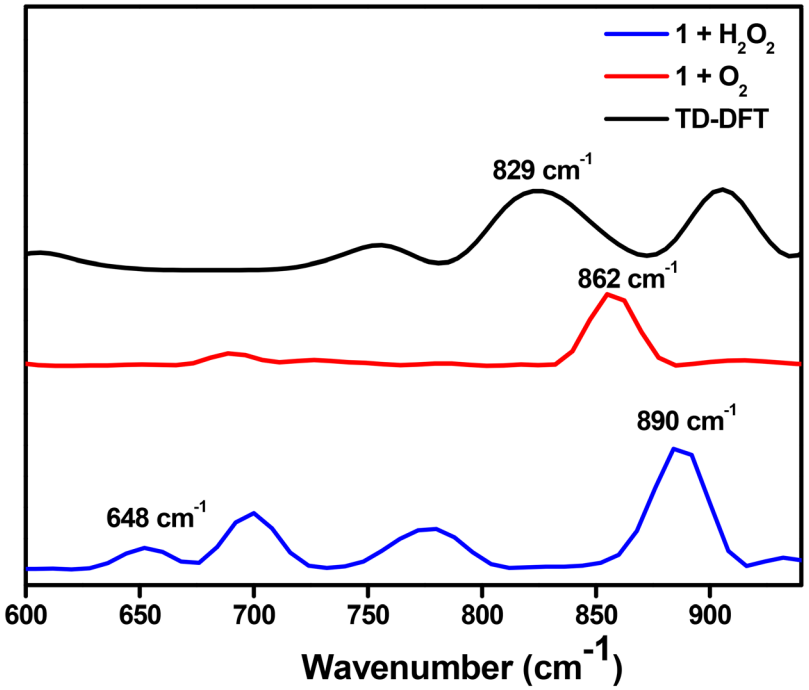

Fig. 3 Vibrational spectra of Cu(II)–peroxo species (blue) generated from **1** (1×10^{-4} M) by adding 10 equivalents of H_2O_2/Et_3N (2 equivalents) in dry CH_3CN and by adding O_2/Et_3N (2 equiv.) in CH_3CN (red). Calculated vibrational spectra of $[(L)Cu^{II}–OOH]^+$ using TD-DFT (black).

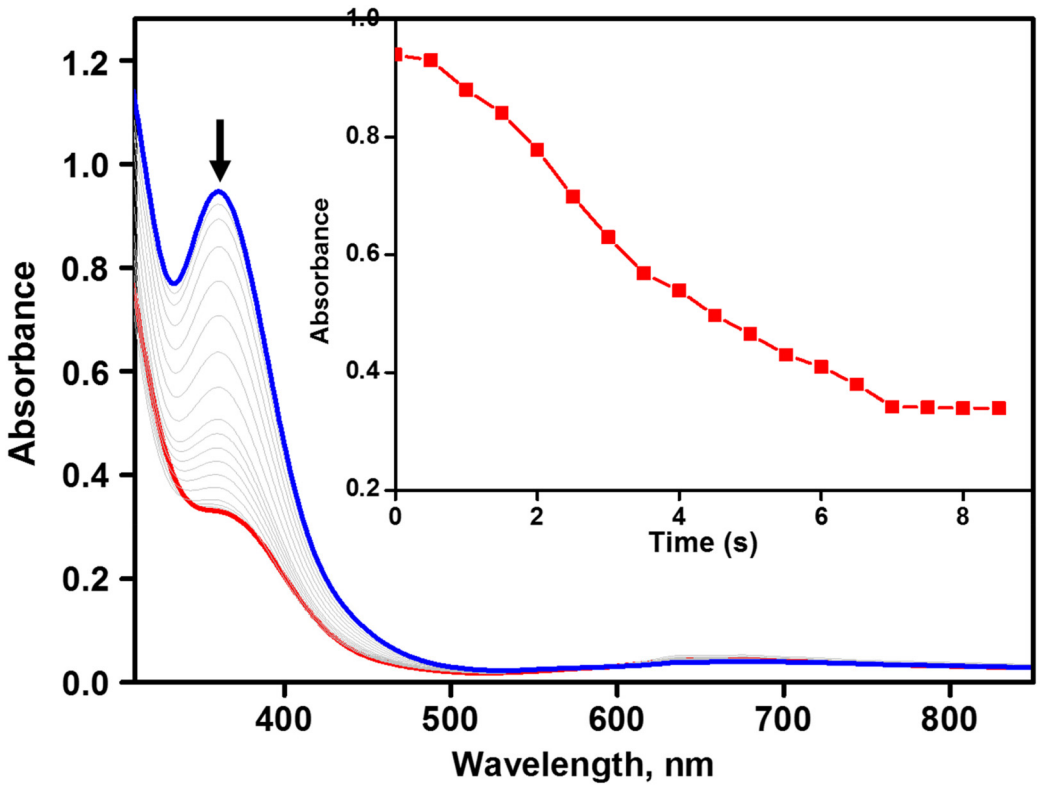

Fig. 4 Electronic spectral changes of the $[(L)Cu^{II}–OOH]^+$ reaction with 50 equivalents of benzene at −20 °C in dry acetonitrile.

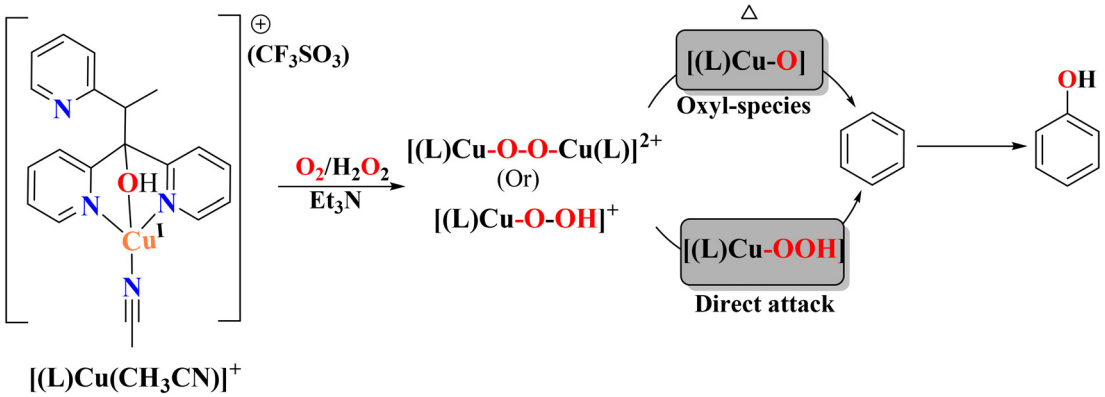

Scheme 3 The proposed mechanism for benzene hydroxylation by complex **1**.

phenol and eliminates the Fenton-type reaction pathway.[60] Cyclohexane as the substrate and CCl_4 as the radical trapping agent showed 96% selectivity for oxidation products of cyclohexanol and cyclohexanone formation with 4% of cyclohexyl chloride, which again supports the exclusion of the radical-type reaction pathway.[35] Using cyclohexanal as the substrate, no deformylation reaction was observed under identical conditions, and the substrate was completely recovered. This result suggests that the aldehyde deformylation reaction *via* nucleophilic attack is not facilitated by the intermediate Cu(II)–peroxo species. The reaction of thioanisole and triphenylphosphine showed the formation of methyl phenyl sulfoxide (56%) and triphenylphosphine oxide (29%), respectively, at 25 °C over 3 h. Thus, this result suggests the electrophilic nature of the key intermediate $[(L)Cu^{II}–OOH]^+$ or $[(L)Cu^{II}–O–O–Cu^{II}(L)]^{2+}$. Similarly, benzene-$d_1$ was employed as a substrate under identical reaction conditions to understand the mechanism better, and no product formation was observed *via* the NIH shift.[60] Therefore, it is evident that the initial formation of the Cu(II)–peroxo intermediate may either undergo direct electrophilic hydroxylation or be converted into highly reactive copper–oxyl (Cu–O) species. This Cu–O species possibly reacts with the benzene leading to the formation of phenol through an electrophilic mechanism (Scheme 3). Our repeated attempts to isolate single crystals of the $[(L)Cu^{II}–OOH]^+$ or $[(L)Cu^{II}–O–O–Cu^{II}(L)]^{2+}$ species were unsuccessful under various conditions.

However, the geometry of intermediate $[(L)Cu^{II}–OOH]^+$ species was optimized using ORCA 4.0 (Fig. 5).[61] The calculations were performed using B3LYP and def2-TZVP, def2/J basis sets.[62,63] The calculated bond distances of Cu–O (1.830 Å) and O–O (1.383 Å) are close to those of previously reported intermediates (Cu–O, 1.888 Å; O–O, 1.460 Å).[35,55] The calculated electronic spectra of $[(L)Cu^{II}OOH]^+$ by TDDFT showed O (π^*_σ) → Cu^{2+} LMCT at 429 nm (Fig. S19†), which is closer to the experimental value (360 nm). Furthermore, this preliminary DFT optimization indicates that the coordination of the remaining pyridine pendant is likely to destabilize the intermediate Cu^{II}–OOH species. The calculated vibration

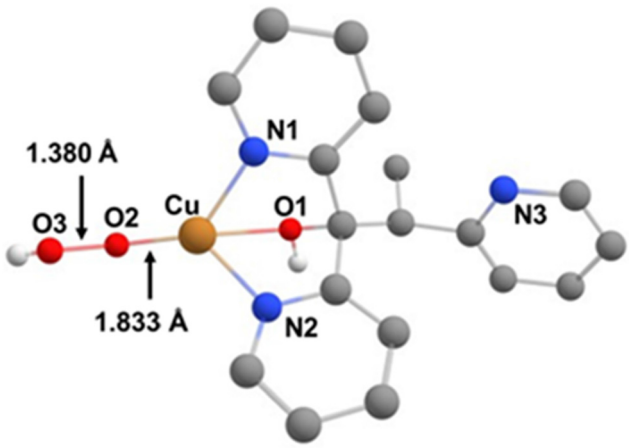

Fig. 5 Optimized structure of $[(L)Cu^{II}–OOH]^+$ using the hybrid density functional B3LYP and a double-zeta quality split valence basic set with polarization functions (def2-SVP), and the geometry was optimized using longer triple-zeta basis sets (def2-TZVP) for all atoms.

spectra showed O–O and Cu–O stretching frequencies at 829 cm^{-1} and 606 cm^{-1}, which are comparable to our experimental data (Fig. 3).[35]

Conclusions

A new tris-pyridine-based mononuclear copper complex **1** was synthesized and characterized as a relevant model for copper monooxygenase. It afforded a dicopper(II) complex **2** *via* typical aerial oxidation with the protonation of one of the pyridyl arms of the ligand. Complex **3** was generated by a separate reaction, and ligand coordination was observed without protonating the pyridyl arms. Single-crystal XRD analysis of dicopper complexes **2** and **3** confirmed the above observation. Both the dicopper complexes showed distorted square pyramidal geometry, and their Cu–Cu distances in both cases were almost identical (2.9 Å). Benzene hydroxylation was performed using copper complexes; copper(I) complex **1** showed the con-

version of benzene to phenol (7%) as the sole product at 60 °C under an O_2 atmosphere over 48 hours. The phenol yield increased to 19% using H_2O_2 as the oxidizing agent within 8 hours. However, dicopper complexes showed no conversion under O_2 and relatively poor phenol conversion with H_2O_2 (4–6%). The electronic, vibrational, and mass spectroscopy results support that the hydroxylation reaction mechanism proceeds *via* Cu(II)–peroxo species. DFT and TD-DFT calculation results are comparable to the experimental data. The KIE investigations further support the involvement of Cu–oxygen species. The structural, spectral, and magnetic properties of **2** and **3** are in progress for a better understanding of them.

Experimental section

Materials

The chemicals di-2-pyridylketone, 2-ethylpyridine, *n*-BuLi in cyclohexane $[Cu^{I}(CH_3CN)_4]CF_3SO_4$, $[Cu^{II}(CF_3SO_4)_2]$, tetrabutylammonium hexafluorophosphate, benzene, chloroform-*d*, benzene-d_6, chlorobenzene, nitrobenzene, and toluene were purchased from Sigma-Aldrich and $H_2{}^{18}O_2$ (90% ^{18}O atom) was purchased from Icon Isotope. Anhydrous acetonitrile, dichloromethane, and hydrogen peroxide (30%) from Merck, India. Dry methanol and phenol were purchased from SD Fine Chemicals.

Experimental conditions and physical measurements

All workup procedures were conducted under ambient conditions. All NMR spectra were recorded on a Bruker 300 MHz spectrometer. Chemical shift values are given in parts per million (ppm). Electrospray ionization (ESI-MS) was measured on a Thermo LC-MS instrument. UV-Vis spectra were recorded on an Agilent 8453 spectrometer with a cooling unit by Unisoku (Osaka, Japan). Cyclic Voltammetry (CV) was performed using a three-electrode cell configuration. A platinum sphere (acetonitrile medium), glassy carbon (non-aqueous), platinum wire, and Ag(s)/Ag^+ were used as the working, auxiliary, and reference electrodes, respectively. The tetrabutylammonium hexafluorophosphate was used as a supporting electrolyte in acetonitrile. GC-MS and GC analyses were performed on an Agilent 5977E GCMSD using an HP-5 MS ultra-inert (30 m × 250 μm × 0.25 μm) capillary column.

Single-crystal X-ray structure analysis

The experiment was performed on an Agilent Technologies Supernova-E CCD diffractometer. The single crystals of 2 and 3 with suitable sizes were selected from the mother liquor, immersed in paraffin oil, and then mounted on the tip of glass fiber. The structures were solved using the direct methods of the SHELXS-2013 program. Refinement and all further calculations were carried out using SHELXL-2013. The H atoms were included in calculated positions and treated as riding atoms using the SHELXL default parameters. The non-H atoms were refined anisotropically, using weighted full-matrix least-squares on F^2. CCDC 1962712 and 1962738† contain the supplementary crystallographic data for this paper.

Synthesis of the ligand

The ligand (L) was synthesized using the following procedure: a solution of *n*-BuLi (7 mL, 14.0 mmol of 2 M in hexane) was added dropwise *via* a syringe over 15 minutes to 2-ethylpyridine (1.6 mL, 12.0 mmol), which was pre-cooled to −78 °C in dry THF (40 mL) under an argon atmosphere. Then, the mixture was stirred vigorously at a temperature below −70 °C. After 30 minutes, the solution turned deep red, and di(2-pyridyl)ketone (1.1 g, 6 mmol) in THF (10 mL) was added while maintaining the temperature below −65 °C. The solution was further stirred for another 3 hours. Finally, the reaction was quenched with water at 0 °C, and the organic layer was extracted using ethyl acetate. The solvent was removed using a rotary evaporator to form a solid with a yellow oil compound. Off-white crystalline solids were obtained by passing through silica column chromatography (7 : 3, hexane : ethyl acetate) with a yield of 69% (1.2 g). HRESI-MS (*m*/*z*): 290.14 $[M - 1]^-$. ^1H NMR (300 MHz, $CDCl_3$), δ in ppm, 8.63 (d, 1H), 8.36 (d, 1H), 8.29 (d, 1H), 8.01 (d, 1H), 7.79 (d, 1H), 7.68 (t, 1H), 7.45 (q, 2H), 7.33 (d, 1H), 7.14 (d, 1H), 6.96–6.88 (dt, 2H), 4.78 (q, 1H) and 1.19 (d, 3H). ^{13}C NMR ($CDCl_3$), 164.41, 157.66, 148.66, 126.57, 125.31, 63.61, 60.24, 58.01, 54.48, 27.48, 13.61, 11.31 ppm. Anal. calcd for $C_{18}H_{17}N_3O$: C, 74.20; H, 5.88; N, 14.42; found: C, 74.19; H, 5.93; N, 14.38.

Synthesis of copper complexes

To a toluene/acetone (1.5 mL/0.5 mL) solution of $[Cu^{I}(CH_3CN)_4]CF_3SO_3$ (0.0375 g, 0.1 mmol), L1 of (0.029 g, 0.1 mmol) in a toluene/acetone (1.8 mL/0.2 mL) was added and stirred for 2 hours under an Ar atm. Then, 15 mL of degassed diethyl ether was added and stirred for an hour. A yellowish-white precipitate settled down, corresponding to copper(I) complex **1** (0.04 g, yield 74%). This complex is highly air-sensitive.

$[Cu^{I}(L)(CH_3CN)]CF_3SO_3$ (1). HRESI-MS (*m*/*z*): 354.0671 $[M - CH_3CN]^+$; ^1H NMR (300 MHz, $CDCl_3$), 7.31 (d, 8H), 6.75 (d, 4H), 1.20 (m, 4H). Anal. calcd for $C_{21}H_{20}CuF_3N_4O_4S$: C, 46.28; H, 3.70; N, 10.28; found: C, 46.30; H, 3.74; N, 10.25.

$[(Cu^{II}L)(Cu^{II}L\ H)(SO_3CF_3)_2]\cdot CF_3SO_3\cdot H_2O$ (2). Furthermore, complex **1** was dissolved in CH_3CN/diethyl ether and maintained for recrystallization, leading to the formation of a copper(II) complex (**2**). HRESI-MS (*m*/*z*): 758.8621 $[M - (CF_3SO_3)_3 + H_2O + CH_3OH]^+$. Anal. calcd for $C_{39}H_{33}Cu_2F_9N_6O_{11}S_3$: C, 40.52; H, 2.88; N, 7.27; found: C, 40.50; H, 2.90; N, 7.28.

$[(LCu^{II})_2(SO_3CF_3)_2]$ (3). To a $Cu^{II}(CF_3SO_3)_2$ (0.072 g, 0.2 mmol) in acetonitrile, the ligand (0.058 g, 0.2 mmol) in acetonitrile was added dropwise, and the solution was stirred for 2 hours. The formed violet-colored solution was kept for crystallization. The long-standing solution at room temperature afforded single crystals suitable for X-ray diffraction (XRD) analysis. Yield (0.10 g, 58%). HRESI-MS (*m*/*z*): 855.03 [M –

$CF_3SO_3]^+$. Anal. calcd for $C_{38}H_{32}Cu_2F_6N_6O_8S_2$: C, 45.37; H, 3.21; N, 8.35; found: C, 45.39; H, 3.22; N, 8.31.

General procedure for the catalytic hydroxylation reaction

A catalytic amount of complex **1** (0.05 mmol) was dissolved in dry acetonitrile (3.0 mL). Triethylamine (5.0 mmol) and benzene (5.0 mmol) were introduced slowly into the solution. Under O_2, the reaction mixture was stirred at 60 °C/25 °C for 48 hours. After cooling to room temperature, the catalyst or trimethylamine *N*-oxide was removed by passing the mixture through a silica gel column. Then, the solution was analyzed and quantified by GC-MS/GC using a known concentration of nitrobenzene, which was added as an internal standard. The conversion and yield of the reaction were determined using GC-MS/GC. Instead of O_2, 30% hydrogen peroxide (2.5 mL, 25 mmol) was used as an oxygen source for a few catalytic reactions. The control experiment without a catalyst showed no benzene oxidation products under identical experimental conditions. Here, the yields were calculated based on the starting substrates.

Determination of the kinetic deuterium isotope effect

Benzene (0.25 mmol), benzene-d_6 (0.25 mmol), and triethylamine (0.25 μmol) were added to a solution of **1** (0.025 mmol) in dry acetonitrile (3 mL). Aqueous hydrogen peroxide (30%) (5 mmol, 0.50 mL) was then added slowly under constant stirring. The mixture was stirred for 24 hours at 60 °C. After cooling to room temperature, the catalyst was removed by passing the mixture through a silica gel column, then the solution was analyzed, and the product distribution was determined by GC-MS/GC. The kinetic isotope effect (KIE) value for phenol production was calculated using the formula: (moles of phenol)/(moles of phenol-d_5).

Catalytic benzene hydroxylation reaction with $H_2{}^{18}O_2$

Complex **1** (2.5 μmol) was dissolved in dry acetonitrile and benzene (0.12 mmol). Then, triethylamine (0.12 mmol) and $H_2{}^{18}O_2$ (5 equivalents) were slowly added to the reaction mixture. The mixture was stirred for 10 hours at 60 °C. After cooling to room temperature, the catalyst was removed by passing the mixture through a silica gel column, and then the solution was analyzed and quantified by GC-MS/GC.

Catalytic benzene hydroxylation reaction with $H_2{}^{18}O$

Complex **1** (2.5 μmol) was dissolved in $H_2{}^{18}O$/acetonitrile (0.1 mL/1 mL). Triethylamine (0.12 mmol), benzene (0.12 mmol) and aqueous hydrogen peroxide (0.5 mL, 5 mmol) were slowly introduced into the solution. The reaction mixture was stirred at 60 °C for 8 hours. After cooling to room temperature, the catalyst was removed by passing the mixture through a silica gel column, and then the solution was analyzed and quantified by GC-MS/GC.

Catalytic hydroxylation of substituted benzene

The most active catalyst **1** (0.05 mmol) was dissolved in dry acetonitrile (3.0 mL). Triethylamine (5.0 mmol), the substrate (5.0 mmol), and aqueous hydrogen peroxide (2.5 mL, 25 mmol) were slowly added to the solution. The reaction mixture was stirred at 60 °C for 8 hours. The same procedure was employed for the reaction with O_2, where **1** was dissolved in acetonitrile. After cooling to room temperature, the catalyst was removed by passing the mixture through a silica gel column, and the products were analyzed by GC-MS/GC.

Kinetic measurements

Kinetic experiments for the formation of Cu(II)–peroxo species were carried out in a 1 cm path length UV-visible cell on a Unisoku thermostated cell holder, designed for low-temperature measurements. The deaerated solution of the copper complexes (1×10^{-4} M) in the cell was maintained at the desired temperature for several minutes, and the oxidant (aqueous 30% H_2O_2 (10 equivalents)) was added *via* a microsyringe in acetonitrile. The formation of the intermediates was determined by time-dependent UV-visible spectroscopy.

DFT methods

The geometry optimizations were performed using density functional theory (DFT) methods. DFT calculations were carried out using the hybrid density functional B3LYP and a double-zeta quality split valence basic set with polarization functions (def2-SVP),[35] and the geometry was optimized using longer triple-zeta basis sets (def2-TZVP)[35] for all atoms, and TD-DFT calculations were also performed using B3LYP and basic set def2-TZVP[35] for all atoms. All DFT calculations were carried out using the Orca 4.0 program.[61]

Data availability

Supplementary data associated with this article can be found in the ESI† on the journal homepage.

Conflicts of interest

There are no conflicts to declare.

Acknowledgements

We acknowledge the Science and Engineering Research Board (SERB), New Delhi (CRG/2020/003016), for funding, and RR thanks the CSIR, New Delhi, for the senior research fellowship (09/201(0426)/2019-EMR-I).

References

1 N. Herron and C. A. Tolman, *J. Am. Chem. Soc.*, 1987, **109**, 2837.
2 T. Kitano, Y. Kuroda, M. Mori, S. Ito, K. Sasaki and M. Nitta, *J. Chem. Soc., Perkin Trans. 2*, 1993, 981.

3 Y. Liu, K. Murata and M. Inaba, *J. Mol. Catal. A: Chem.*, 2006, **256**, 247.
4 E. E. Chufan, S. C. Puiu and K. D. Karlin, *Acc. Chem. Res.*, 2007, **40**, 563.
5 H. Hock and S. Lang, *Ber. Dtsch. Chem. Ges. A, B*, 1944, **77**, 257.
6 D. Bianchi, R. D'Aloisio, R. Bortolo and M. Ricci, *Appl. Catal., A*, 2007, **327**, 295.
7 X. Q. Wang, J. P. Wu, M. W. Zhao, Y. F. Lv, G. Y. Li and C. W. Hu, *J. Phys. Chem. C*, 2009, **113**, 14270.
8 J.-F. Bartoli, V. Mouries-Mansuy, K. Le Barch-Ozette, M. Palacio, P. Battioni and D. Mansuy, *Chem. Commun.*, 2000, 827.
9 P. Roy, K. Dhara, M. Manassero and P. Banerjee, *Eur. J. Inorg. Chem.*, 2008, **28**, 4404.
10 P. K. Tandon, R. Baboo, A. K. Singh, G. Purwar and M. Purwar, *Appl. Organomet. Chem.*, 2005, **19**, 1079.
11 A. Marsella, S. Agapakis, F. Pinna and G. Strukul, *Organometallics*, 1992, **11**, 3578.
12 L. V. Pirutko, V. S. Chernyavsky, A. K. Uriarte and G. I. Panov, *Appl. Catal., A*, 2002, **227**, 143.
13 A. Costine, T. O'Sullivan and B. K. Hodnett, *Catal. Today*, 2005, **99**, 199.
14 K. Weissermehl and H. J. Arpe, *Industrielle Organische Chemie*, VCH, Weinheim, 1997.
15 C. Citek, B. L. Lin, T. E. Phelps, E. C. Wasinger and T. D. Stack, *J. Am. Chem. Soc.*, 2014, **136**, 14405.
16 R. Balasubramanian, S. M. Smith, S. Rawat, L. A. Yatsunyk, T. L. Stemmler and A. C. Rosenzweig, *Nature*, 2010, **465**, 115.
17 W. Kaim and J. Rall, *Angew. Chem., Int. Ed.*, 1996, **35**, 43.
18 J. P. Klinman, *Chem. Rev.*, 1996, **96**, 2541.
19 J. P. Klinman, *J. Biol. Chem.*, 2006, **281**, 3013.
20 P. Chen and E. I. Solomon, *Proc. Natl. Acad. Sci. U. S. A.*, 2004, **101**, 13105.
21 S. Itoh and S. Fukuzumi, *Acc. Chem. Res.*, 2007, **40**, 592.
22 E. I. Solomon, D. E. Heppner, E. M. Johnston, J. W. Ginsbach, J. Cirera, M. Qayyum, M. T. Kieber-Emmons, C. H. Kjaergaard, R. G. Hadt and L. Tian, *Chem. Rev.*, 2014, **114**, 3659.
23 J. S. Woertink, P. J. Smeets, M. H. Groothaert, M. A. Vance, B. F. Sels, R. A. Schoonheydt and E. I. Solomon, *Proc. Natl. Acad. Sci. U. S. A.*, 2009, **106**, 18908.
24 E. I. Solomon, *Inorg. Chem.*, 2016, **55**, 6364.
25 J. M. Bollinger Jr., *Nature*, 2010, **465**, 40.
26 S. Schindler, *Eur. J. Inorg. Chem.*, 2000, **11**, 2311.
27 Y. R. Luo, *Comprehensive Handbook of Chemical Bond Energies*, 1999, p. 1.
28 P. Zhai, L. Wang, C. Liu and S. Zhang, *Chem. Eng. J.*, 2005, **111**, 1.
29 M. Becker, S. Schindler, K. D. Karlin, T. A. Kaden, S. Kaderli, T. Palanché and A. D. Zuberbühler, *Inorg. Chem.*, 1999, **38**, 1989.
30 H. R. Lucas, L. Li, A. A. Sarjeant, M. A. Vance, E. I. Solomon and K. D. Karlin, *J. Am. Chem. Soc.*, 2009, **131**, 3230.
31 A. Conde, M. M. Diaz-Requejo and P. J. Perez, *Chem. Commun.*, 2011, **47**, 8154.
32 L. Vilella, A. Conde, D. Balcells, M. M. Diaz-Requejo, A. Lledos and P. J. Perez, *Chem. Sci.*, 2017, **8**, 8373.
33 E. Borrego, L. Tiessler-Sala, J. J. Lazaro, A. Caballero, P. J. Perez and A. Lledos, *Organometallics*, 2022, **41**, 1892.
34 T. Tsuji, A. A. Zaoputra, Y. Hitomi, K. Mieda, T. Ogura, Y. Shiota, K. Yoshizawa, H. Sato and M. Kodera, *Angew. Chem., Int. Ed.*, 2017, **56**, 7779.
35 S. Muthuramalingam, K. Anandababu, M. Velusamy and R. Mayilmurugan, *Inorg. Chem.*, 2020, **59**, 5918.
36 (*a*) S. Kumari, S. Muthuramalingam, A. K. Dhara, U. P. Singh, R. Mayilmurugan and K. Ghosh, *Dalton Trans.*, 2020, **49**, 13829; (*b*) R. Ramasubramanian, K. Anandababu, N. C. Mösch-Zanetti, F. Belaj and R. Mayilmurugan, *Dalton Trans.*, 2019, **48**, 14326; (*c*) K. Anandababu, R. Ramasubramanian, H. Wadepohl, P. Comba, N. Britto, M. Jaccob and R. Mayilmurugan, *Chem. – Eur. J.*, 2019, **25**, 9540.
37 C. H. Kjaergaard, S. M. Jones, S. Gounel, N. Mano and E. I. Solomon, *J. Am. Chem. Soc.*, 2015, **137**, 8783.
38 S. H. Laurie, T. Lund and J. B. Raynor, *J. Chem. Soc., Dalton Trans.*, 1975, **14**, 1389.
39 B. J. Hathaway and A. Tomlinso, *Coord. Chem. Rev.*, 1970, **5**, 1.
40 U. Sakaguchi and A. W. Addison, *J. Chem. Soc., Dalton Trans.*, 1979, **4**, 600.
41 A. W. Addison, T. N. Rao, J. Reedijk, J. van Rijn, G. C. Verschoor and J. Chem, *Soc., Dalton Trans.*, 1984, **7**, 1349.
42 T. Tsukihara, H. Aoyama, E. Yamashita, T. Tomizaki, H. Yamaguchi, K. Shinzawa-Itoh, R. Nakashima, R. Yaono and S. Yoshikawa, *Science*, 1995, **269**, 1069.
43 S. Iwata, C. Ostermeier, B. Ludwig and H. Michel, *Nature*, 1995, **376**, 660.
44 M. Wilmanns, P. Lappalainen, M. Kelly, E. Sauer-Eriksson and M. Saraste, *Proc. Natl. Acad. Sci. U. S. A.*, 1995, **92**, 11955.
45 R. P. Houser, V. G. Young and W. B. Tolman, *J. Am. Chem. Soc.*, 1996, **118**, 2101.
46 J. M. Bollinger Jr, *Nature*, 2010, **465**, 40.
47 C. W. Koo, F. J. Tucci, Y. He and A. C. Rosenzweig, *Science*, 2022, **375**, 1287.
48 V. C. Wang, S. Maji, P. P. Chen, H. K. Lee, S. S. Yu and S. I. Chan, *Chem. Rev.*, 2017, **117**, 8574.
49 (*a*) P. L. Holland, K. R. Rodgers and W. B. Tolman, *Angew. Chem., Int. Ed.*, 1999, **38**, 1139; (*b*) S. P. de Visser, K. Oh, A.-R. Han and W. Nam, *Inorg. Chem.*, 2007, **46**, 4632; (*c*) P. Heim, R. Gericke, G. Spedalotto, M. Lovisari, E. R. Farquhar and A. R. McDonald, *Dalton Trans.*, 2023, **52**, 2663.
50 R. Augusti, A. O. Dias, L. L. Rocha and R. M. Lago, *J. Phys. Chem. A*, 1998, **102**, 10723.
51 (*a*) Q. Xing, H. Lv, C. Xia and F. Li, *Chem. Commun.*, 2016, **52**, 489; (*b*) M. Yamada, K. D. Karlin and S. Fukuzumi,

Chem. Sci., 2016, **7**, 2856; (*c*) Y. Yamada, C.-M. Teoh, Y. Toyoda and K. Tanaka, *New J. Chem.*, 2022, **46**, 955–958.
52 K. Ohkubo, T. Kobayashi and S. Fukuzumi, *Angew. Chem., Int. Ed.*, 2011, **50**, 8652.
53 B. Kim, D. Jeong and J. Cho, *Chem. Commun.*, 2017, **53**, 9328.
54 D. Maiti, H. R. Lucas, A. A. Sarjeant and K. D. Karlin, *J. Am. Chem. Soc.*, 2007, **129**, 6998.
55 B. Kim, D. Jeong, T. Ohta and J. Cho, *Commun. Chem.*, 2019, **2**, 81.
56 M. Kodera, T. Kita, I. Miura, N. Nakayama, T. Kawata, K. Kano and S. Hirota, *J. Am. Chem. Soc.*, 2001, **123**, 7715.
57 C. Wurtele, O. Sander, V. Lutz, T. Waitz, F. Tuczek and S. Schindler, *J. Am. Chem. Soc.*, 2009, **131**, 7544.
58 M. S. Reynolds and A. Butler, *Inorg. Chem.*, 1996, **35**, 2378.
59 L. Gomez, I. Garcia-Bosch, A. Company, J. Benet-Buchholz, A. Polo, X. Sala, X. Ribas and M. Costas, *Angew. Chem., Int. Ed.*, 2009, **48**, 5720.
60 (*a*) K.-B. Cho, X. Wu, Y.-M. Lee, Y. H. Kwon, S. Shaik and W. Nam, *J. Am. Chem. Soc.*, 2012, **134**, 20222; (*b*) J. T. Groves, *J. Chem. Educ.*, 1985, **62**, 928; (*c*) J. T. Groves and T. E. Nemo, *J. Am. Chem. Soc.*, 1983, **105**, 6243.
61 F. Neese, *Comput. Mol. Sci.*, 2018, **8**, e1327.
62 A. Schäfer, H. Horn and R. Ahlrichs, *J. Chem. Phys.*, 1992, **97**, 2571.
63 F. Weigend and R. Ahlrichs, *Phys. Chem. Chem. Phys.*, 2005, **7**, 3297.